Effectivity of a bubble screen as separator of waters of different densities

Master of Science

Internship technical report

by

Lina Nikolaidou

Contents

1 Introduction

1.1. Problem statement

Bubble screens are applied in shipping locks located between sea and freshwater canals. They act as a barrier that helps reduce the amount of salt through the lock every locking cycle. The intrusion of salt water into fresh water poses a threat to the fresh water systems. Those inland waters are used for agriculture and drinking water purposes, so that their allowable salt concentration is quite strict. Furthermore, there is an ecological importance regarding the water quality of inland water bodies. With heavier traffic and ever larger shipping locks being built (the new Ijmuiden lock being the world's largest), the limits set on salt intrusion are a real challenge for lock engineers.

Various recent researches performed, show the effectiveness of bubble screens as a measure that slows down salt intrusion. Some of these studies consider not only bubble screens, but also the (additional) implementation of a discharge of fresh water flushing the lock chamber and of so-called water screens (1.1). The required amount of electrical power, and the costs of installing large air compressors are the motivation for a desired optimization of the bubble screen application.

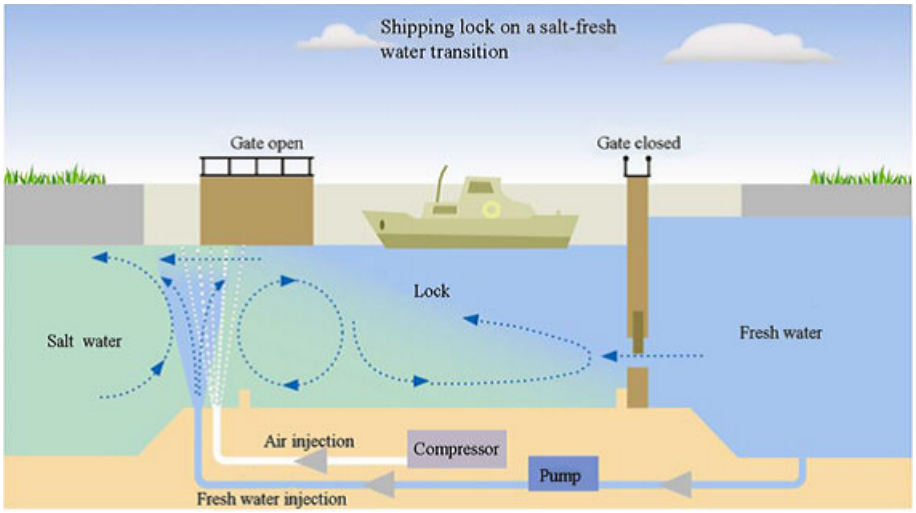

Figure 1.1: Shipping lock, water screen and bubble screen (Keetels et al., 2011)

However, it is unclear why the bubble screens work the way they do and how their performance could be optimized. Various physical phenomena play a role in this bubble screen application: bubbly induced flow, mixing, pressures due to density differences and the induced water movement.

1.2. Objectives

A bubble screen can reduce the propagation time of the salt water front, but it cannot stop it. The effectiveness of the bubble screen has been estimated using theoretical approximations. However it is still unclear how the theory holds for different flow specifications and lock dimensions.

To that end it is within the objectives of that project, to increase the understanding of bubble screens, so that their range of applicability can be extended.

In more recent years, the modelling of gas-liquid flows using CFD has been widely studied. Quite a big amount of work has been done on modelling bubble columns compared with little to no work for the bubble screens. Nevertheless, a CFD model accurately resolving the fluid dynamics of this application could be used to extrapolate the theory to different geometries.

1.3. Research questions

As far as the bubble screens are concerned there are a lot of questions still to be answered. In the present study, the main research question addresses CFD modelling and more specifically, if it possible to simulate bubbly driven flows with CFD effectively and validate the modelling results with experimental ones. However, being able to simulate such flows efficiently demands detailed study on the underlying physics of the processes involved.

That being said, some other research questions addressed in the present study refer to the bubbly flow itself. One also important aspect, briefly addressed, is the scalability of such flows and the dimensionless number theory involved.

2

Literature Review

2.1. Preface

To be able to understand why bubble screens in shipping locks work the way they do, one has to understand the physics of density driven flow and also explain the behavior of bubble curtains. The topic of exchange flow is well-covered by the literature, whereas literature on bubbly driven flow combined with density currents is limited.

Effectively modelling exchange flow with CFD is also something that has been studied and results are available. Including a bubble screen in the simulations is something relatively new, which introduces difficulties and additional effects.

2.2. TKI Project

This research was performed as part of the TKI research project "Effectiviteit van een bellenscherm als scheider van water van verschillende dichtheden" ("Effectivity of a bubble screen as separator of waters of different densities"). The project was granted by the TKI Deltatechnologie on April 19th, 2017. It is therefore decided to initiate the literature review with a summary of the work already conducted within the project and then proceed to the next chapter, highlighting the contribution of the present study to the current knowledge.

The goal of the TKI project is:

- To increase the available knowledge regarding bubble screen technology as separator of waters of different densities
- To assess the validity of scale model measurements as research method to estimate the effectiveness of this bubble screen application

To that end, two types of experiments were performed:

- Detailed PIV (particle image velocimetry) measurements of the flow velocities induced by a bubble screen, considering a steady state
- Measurements recording the concentration of dye to quantitatively measure the mixing of water from both sides of the bubble screen, with or without density difference

Both measurements considered an identical geometry and provided sufficient data to allow a quantitative comparison of several scenarios and validation of CFD computations.

In the following, the aspects of the experiments needed for the CFD validation will be presented shortly.

2.2.1. Experimental set-up

The inner dimensions of the provided water tank measured 2.40 m in length, 0.50 m in width and 0.70 m in height (2.1). The bubble screen generator was place in the middle of the tank, separating the left (lock side) from the right (sea side).

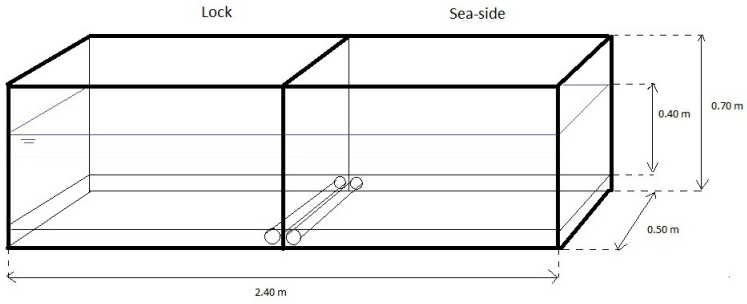

Figure 2.1: Geometry of the tank. The bubble generators are represented by the cylindrical elements at the bottom of the tank towards the middle, on both sides of the gate

Both experiments had been performed simultaneously in close cooperation. The water depth was set to 40cm. Both tanks used are depicted in figures 2.2 and 2.3.

Figure 2.2: Tank used in PIV measurements

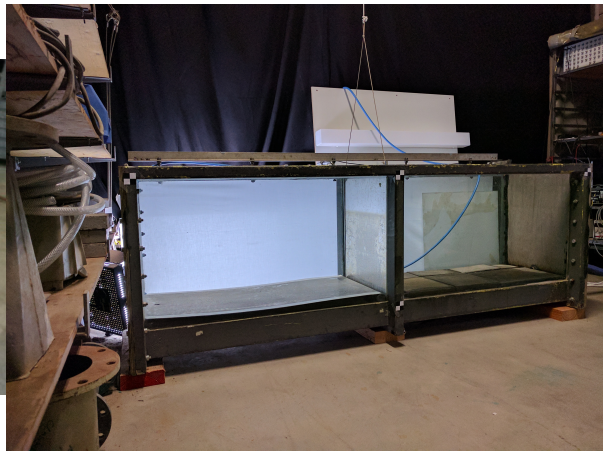

Figure 2.3: Tank used in dye measurements

To study the effect of the bubble size two types of bubble generators were tested. One of them was a simple PVC tube with small holes and the other was a porous air stone like the ones used in aquariums. Because of the necessity to insert a door in the middle for the dye measurements, two strings of bubble generators were made and placed into the flume.

Two PVC tubes were located parallel to each other with spacing of 7.5 cm., and were 50 cm long. They had an outer diameter of 4.0 cm and a wall thickness of 3.2 mm. To create bubbles with a diameter between 3 and 8 mm, tubes of 90 holes each with a diameter of 0.8 mm were used (2.4 and 2.5).

The air stone used had a length of 24.6 cm and a width of 2.5 cm. Two stones had been used next to each other for 1 string. The distance between the two rows of air stone was set to 2 cm from stone to stone (2.6 and 2.7).

Since the bubble screen consists of two parallel bubble generators, the air supply was done from both sides. The air was delivered by a local air pressure network available at the facility. The three air flow rates used for the experiments are summarized in the table below (2.1).

Figure 2.4: PVC tube design

Figure 2.5: PVC screen generator close-up

Figure 2.6: Porous stone close-up

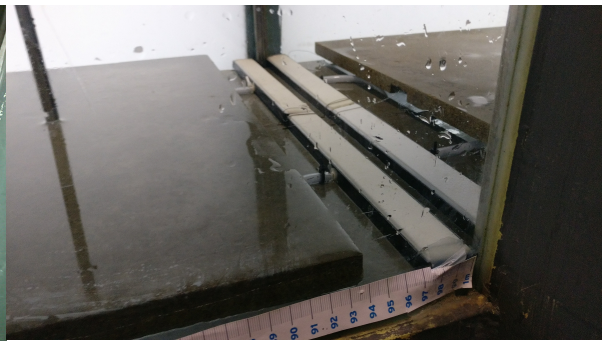

Figure 2.7: Porous stone set-up

Cases	Air flow rate [NL/min]
1	33.50
2	55.96
3	86.86

Table 2.1: Overview of air flow rates

2.2.2. Results of post-processing and analysis of dye measurements

Most of the results of the dye measurements are based on the quantification of the dye amount on the left side of the tank with respect to time. A thorough analysis of the results is available from Kurian (2017). A summary of the results is presented in the following.

The experiment were performed in homogeneous and in-homogeneous water. As can be seen from figure 2.8, in case of homogeneous water, the mixing increases with time, until it reaches a more or less steady condition. Mixing also increases with Fr_{air} number. The Fr_{air} number is an important dimensionless number used to scale the experiments and will be addressed in more detail, later in the literature review. It a function of the air flow rates as summarized in table 2.2. It is defined as:

$$Fr_{air} = \frac{q_a g^{1/3}}{\left(\frac{\Delta\rho}{\rho} g h\right)^{1/2}}$$

Cases	Air flow rate [NL/min]	Fr_{air} number [NL/min]
1	33.50	0.80
2	55.96	0.95
3	86.86	1.10

Table 2.2: Froude air number as a function of air flow rates

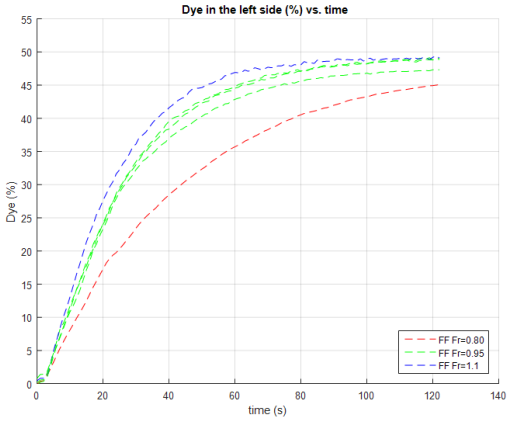

Figure 2.8: Fresh-fresh (FF) cases - left side dye vs. time

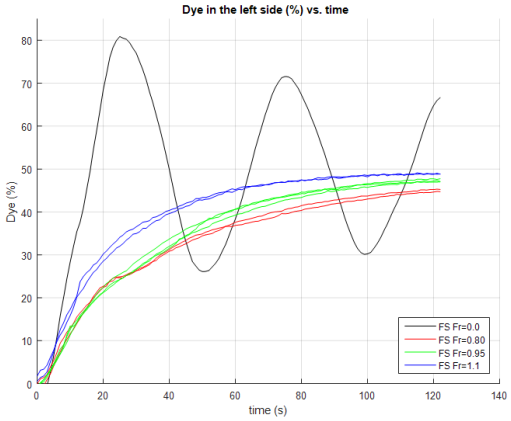

Figure 2.9: Fresh-salt (FS) cases - left side dye vs. time

Fresh-salt (FS) case for different Fr_{air} is shown in figure 2.9. For the case of Fr_{air} 1.1, the transport of dye is increased as compared with the cases with Fr_{air} 0.80 and Fr_{air} 0.95. However,Fr_{air} 0.80 (red) and 0.95 (green) lines appear nearer to each other than with the Fr 1.1 (blue) lines, towards the beginning. The black line represents a simple lock exchange in the absence of a bubble screen (Fr_{air} 0.0).

The study of Kurian (2017) also shows the different mixing mechanisms of the two bubble screen generators for the homogeneous water case. As seen in figure 2.11, for the Fr_{air} 0.80 case, the porous stone bubble generator seems to produce a bubble screen which mixes better than the PVC pipe bubble generator. On the other hand, for the Fr_{air} 0.95 and Fr_{air} 1.1, the PVC bubble screen initially acts as an active separator and later as an active mixer. The transition happens approximately near 40s (2.11).

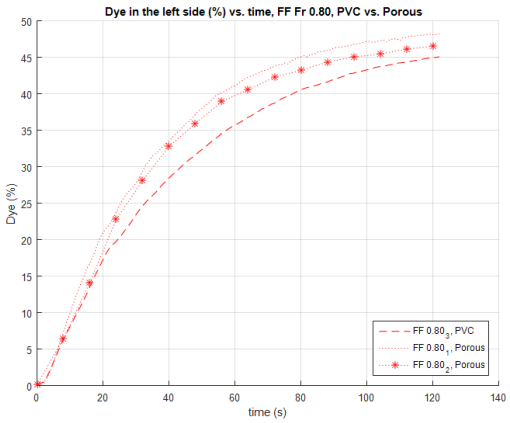

Figure 2.10: Fr_{air} 0.80 PVC pipes vs. porous stones.

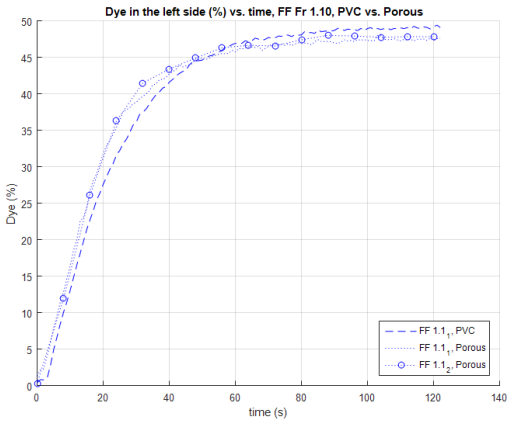

Figure 2.11: Fr_{air} 0.80 PVC pipes vs. porous stones.

2.3. Lock exchange flow and Air Curtain

Basic knowledge to understand density driven flow was already known from course of "Stratified Flows", Pietrzak (2017).

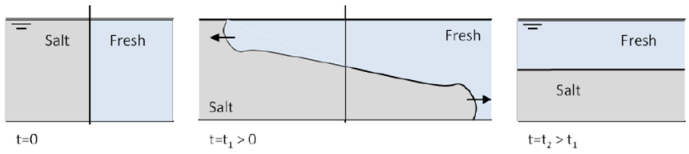

Figure 2.12: Lock-exchange test, source: Lecture slides "Stratified Flows"

Basic aspects of the so-called "Lock exchange test" will be shortly presented. An initial condition of the figure 2.12 is assumed, with the denser water on the left side and the lighter water on the right side. Once the divider is removed, the denser, heavier fluid will propagate in the left direction, bellow the lighter fresher one. Kelvin-Helmholtz instabilities will be appear in the interface. Stratification will tend to smooth these instabilities and finally a steady state will be reached with the freshwater on top on the salt water.

If we are to consider this phenomenon in a lock, there are some parameters to be taken into account. For example, currents may be induced by the motion of ships that might favor or unfavor the propagation of the density current. Secondly in locks we are not dealing with two closed domain like in the experiment, in the sense that the horizontal dimensions are bigger.

Several articles are concerned with the dynamics of gravity currents. The velocity of the fronts is of great importance and there are different ways in calculating that, in different sources. A systematic way to approximate the velocities based on energy concerning flow is presented in Shin et al. (2004) while Abraham and van der Burgh (1962), presents a different approach, although still dealing with energy considerations.

For the present study, the velocity can be calculated as described in Abraham and van der Burgh (1962), as it also uses the air-Froude number and the theory introduced in deriving this number, namely that the decrease in potential energy due to hydrostatic pressure differences should be equal to the increase in kinetic energy. The result of this calculation roughly corresponds to the speed of the gravity flow, as it can be considered in the salt-saltwater test without the use of a bubble screen.

The main source of information on bubble curtains for the present study came from the Wen and Torrest (1987) and Bulson (1961).

In the work of Wen and Torrest (1987), important concepts in fluid mechanics of aeration-induced circulation are described. The authors measured velocity profiles for different aeration rates and experimental set-ups. Special attention is paid on the surface velocity decay and on the influence of different aeration designs and depths on the circulation patterns. Empirical formulas are provided by the authors can that be proved useful tools for CFD validation.

The article of Bulson (1961), presents a detailed report and analysis of experiments in large scale test. It is a quite old article dealing also with fundamental concepts to extract the results. The investigation here is also targeted on the speed, power and thickness of horizontal currents produced by an air curtain. Conclusions were drawn considering the influence of design characteristics and manifold arrangements on the induced flow.

2.4. Scalling considerations

It also serves the objectives of this study, to investigate scale effects. When dealing with experiments it is inevitable not to consider the origin of the dimensions of the experiment.

The dimensionless number considered for these experiments is the Fr_{air} number:

$$Fr_{air} = \frac{q_a g^{1/3}}{\left(\frac{\Delta\rho}{\rho} g h\right)^{1/2}} \text{ where:}$$

q_a is the air flow rate per unit width of the tank at atmospheric pressure, in $m^3/m/s$

g is the acceleration due to gravity, in m/s^2

ρ is the density of sea water, in kg/m^3

$\Delta\rho$ is the difference in density between salt and fresh water, in kg/m^3

h is the height of the water level, in m.

It is used such that:

$Fr_{air,model} = Fr_{air,prototype}$

It was concluded from practice that an air bubble screen works in an efficient way for Fr_{air} in the range of 0.8-1.2. The maximum $Fr_{air} = 1.1$, was a result of the limited air flow rate that the facility could provide.

The derivation of this dimensionless number was first introduced by Abraham and van der Burgh (1962) and is based on his assumptions that the the loss of potential energy from the salt water is equal to the kinetic energy when the water bodies start to move. He subsequently calculated the amount of energy needed to reduce salt intrusion and the corresponding energy supply by the pneumatic barrier. He ultimately derived the reduction of salt intrusion of salt water as a function of supply of air, which led to the Fr_{air} number.

The limitations of this number is depicted in the absence of the bubble size in the formula. Nevertheless, it is a tool still used is bubbly flows while not much research on other more suitable numbers is available yet.

Following the Uittenbogaard (2009), from theory and experiments it appears that the reduction in salt penetration by the bubble curtain is determined by the Fr_{air} . Often the same density difference as in prototype is used in the lab. It then follows from the scale rule:

$n_{q_a} = \beta(n_H)^{3/2}$ where:

n_{q_a} is ratio in aeration rate between the prototype and the model

n_H is ratio in water depth between the prototype and the model

Factor β should be one, but appears to be smaller because the properties of bubbles are not included.

In the present study β was set equal to one. (Mazijk, 1971) also defines:

$a = \frac{C_{0,proto}}{C_{0,model}}$, so that

$\beta = a^{-3}$

$C_{0,proto}$ is a constant, that gives the entrained flow volume as:

$q_{entr} = C_0(gq_a)^{1/3}h$

Finally C_0 can be calculated from:

$C_1 = \frac{C_0}{4}$, with

$C_1 = (1.1-1.3)1.46(1+\frac{h}{Ho})$, with Ho the the atmospheric pressure in the length of the water column.

C_1 is also involved in the max surface flow velocity induced by the water screen (See (Bulson, 1961) and (Abraham and van der Burgh, 1962)):

$u_{max} = C_1(gq_a)^{1/3}$

In his work, (Mazijk, 1971) to support the case that β is not always one, he used another dimensionless number, defined as the amount of salt into the lock with bubble screen during a normalized period T* in which the door was open divided by the amount of salt into the lock if it was unhindered (no bubble screen), during the same T*.

2.5. CFD modelling of air curtains

Finally, the work of (Van Meerkerk and O'Mahoney, 2014) will be summarized. In this article, a CFD model of a bubble screen is presented and validated with experimental results.

The Euler-Euler method is selected against the Euler-Lagrangian method to simulate the two-phase flow. The possible interface forces to be included in the model are also briefly discussed. These are the drag force, the pressure force, the lift force, the virtual mass force, the turbulent dispersion force and the bubble induced turbulence. The article also highlights the difficulties in modelling turbulence in two-phase flow. More specifically, it addresses the problem of damping the transit character of the flow when using the $k-\epsilon$ model, with the effect being stronger for 2D simulations.

The computational model is also presented in detail by the authors. Finally three different test cases are used to validate the model. The authors concluded that all the computational models were able to reproduce the experimental results on a 3D domain, while in the 2D case, turbulence levels cannot be modeled adequately.

3

Methodological Approach

3.1. PIV post-processing

Post-processing of the PIV measurements, was necessary for the CFD validation. An overview of the set-up of the experiments has already been made. Further details on the set-up and the measuring campaign can be found in Wieleman (2017).

In the PIV technique, two pulses are fired with a short delay in between providing the camera with a double exposed image of the particles in the flow. During the time interval between the pulses the particles have moved a distance which is proportional to their velocities. By further analyzing the acquired image this velocity information is retrieved. To that end, the software DaVis by LaVision was used. The raw double frame images were post-processed and a number of parameters concerning the correlation technique, were prescribed.

Following the work of Wieleman (2017), the domain was divided in three field of views, were images were taken for two different bubble screen generators and three air flow rates. This resulted in a total number of 18 cases.

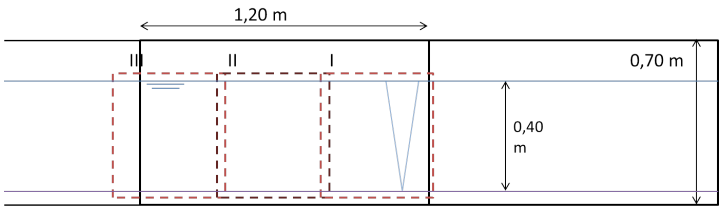

Figure 3.1: PIV frames in the setup

The overlapping coordinates of the three FoVs are presented in the table 3.1.

Mapping	Region 1	Region 2	Region 3
From region 1 to 2	-3.1cm	37.7cm	-
From region 2 to 3	-	4cm	44.7cm

Table 3.1: Overlapping coordinates

Regarding the post-processing parameters, the most important rules are:

- 10 particles are needed per interrogation area
- Maximum particle displacement should be equal to 25% of the interrogation area

- Target percentage of valid vectors equals 95%

Region II was proved to have the better results, while region III was considered the must challenging case. An overview of the setting both for the PVC screen generator and for the porous stones is presented below.

FoV	Airflow rate (NL/min)	No. of frames	Type	Frequency (Hz)	dt (ms)	Interrogation area size
2	33.50	1000	Double	1	5.74596	32×32
2	55.96	1000	Double	1	5.74596	48×48
2	86.86	1000	Double	1	5.74596	48×48
1	33.50	1000	Double	1	5.74596	48×48
1	55.96	1000	Double	1	5.74596	48×48
1	86.86	1000	Double	1	5.74596	48×48
3	33.50	1000 loops of 3	Single	1	1/50s	48×48
3	55.96	1000 loops of 3	Single	1	1/70s	48×48
3	86.86	1000 loops of 3	Single	1	1/70s	48×48

Table 3.2: Overview of post-processing parameters for the Porous stones screen generator

FoV	remove if residual >	re-insert if residual <	delete vector if its peak ration Q<	Min. Number of vectors to compute result
2	2	2.5	2	No
2	5	0	1.2	No
2	5	0	1.2	No
1	2	0	1.5	550
1	2	0	1.5	500
1	3	0	1.2	500
3	5	5	1.2	500
3	5	5	1.2	300
3	5	5	1.2	300

Table 3.3: Overview of post-processing parameters for the Porous stones screen generator

FoV	Airflow rate (NL/min)	No. of frames	Type	Frequency (Hz)	dt (ms)	Interrogation area size
2	33.50	1000 loops of 3	Single	1	1/100s	32×32
2	55.96	1000 loops of 3	Single	1	1/100s	32×32
2	86.86	1000 loops of 3	Single	1	1/100s	32×32
1	33.50	1000	Double	1	5.74596	48×48
1	55.96	1000	Double	1	5.74596	48×48
1	86.86	1000	Double	1	5.74596	48×48
3	33.50	1000 loops of 3	Single	1	1/30s	48×48
3	55.96	1000 loops of 3	Single	1	1/50s	48×48
3	86.86	1000 loops of 3	Single	1	1/80s	48×48

Table 3.4: Overview of post-processing parameters for the PVC screen generator

In terms of computational time, each FoV post-processing lasted approximately 3 hours. Mean velocities and standard deviations were extracted and stored in.txt files.

FoV	remove if residual >	re-insert if residual <	delete vector if its peak ration Q<	Min. Number of vectors to compute result
2	5	0	1	No
2	5	0	1	No
2	5	0	1	No
1	2	0	1.5	550
1	2	0	1.5	550
1	3	0	1.2	550
3	-	-	-	500
3	5	0	1.2	500
3	5	0	1.2	300

Table 3.5: Overview of post-processing parameters for the PVC screen generator

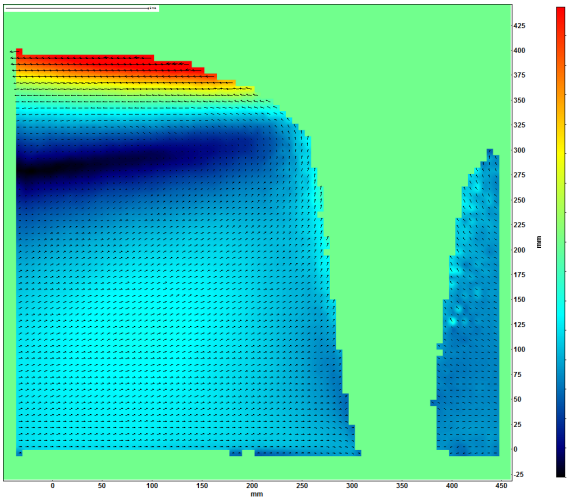

Figure 3.2: Mean velocity vector

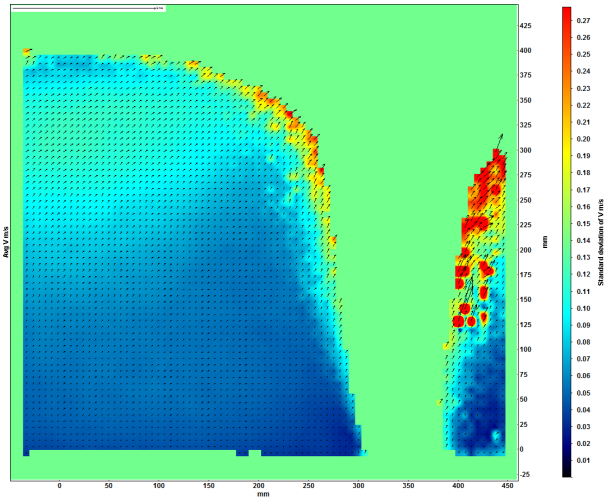

Figure 3.3: Standard deviation of mean velocity vector

3.2. CFD Modelling

3.2.1. Computational model

The computational fluid dynamics model described in this work has been implemented in the commercial CFD package STAR-CCM+, version 12.02.010-R8, made by CD-adapco. The package is a finite volume solver, using staggered grids and a SIMPLE algorithm to solve momentum equations. In the current work the flow is modeled using the Euler-Euler segregated flow solver, following the work already been done (Van Meerkerk and O'Mahoney, 2014).

The interaction between phases only occurs due to interphase forces, with the assumption that there's no mass transfer between phases. The momentum and continuity equations per phase, denoted by the subscript i, are defined as follows:

$$\frac{\partial(a_i \rho_i)}{\partial t} + \nabla(a_i \rho_i v_i) = 0$$

$$\frac{\partial(a_i \rho_i v_i)}{\partial t} + \nabla(a_i \rho_i v_i v_i) = -a_i \nabla p + a_i \rho_i g + \nabla[a_i \tau_i] + M_i$$

With the following necessary conditions:

$$\sum a_i = 1$$

$$\sum M_i = 1$$

In the above equations a_i denotes the volume fraction per phase. In continuity equation, the first term describes the variation of density over time and the second term describes the volume change over space. The first term on the left hand side of momentum equation is the change in velocity and density over time, the second term describes the convection of fluid elements over space. The terms on the right hand side are, respectively, representing the pressure gradient, the effect of gravity, the stress and the interphase momentum transfer due to interface forces. Interphase forces should be equal and opposite.

The instantaneous velocity field is then decomposed in an mean and a fluctuating components. The equations are averaged in time. The resulted RANS equations need a closure model, to determine the viscosity term, included in the shear stress term. In the current work the realizable $k-\epsilon$ model is used for the water phase. The realizable$k-\epsilon$ model is a two equation turbulent viscosity model, based on the standard $k-\epsilon$. For the gas phase, a turbulence response model is used. The turbulence response model predicts velocity fluctuations in the dispersed phase using algebraic correlations to the velocity fluctuations in the continuous phase. The modified $k-\epsilon$ equations are solved for the continuous phase and the turbulence of the dispersed phase is correlated to that of the continuous phase by a response function, determined by the model. In the present work the Tchen turbulence response model provides a dispersed phase turbulent diffusivity for gas flows laden with heavy particles. It is stated by the (Star CCM+, 2018), that is a suitable model for bubbly flows.

In addition, in the transport equations fork_i and ϵ_i, the effect of migrating bubbles on the turbulent kinetic energy and dissipation rate is included by using source terms defined as:

$S_k = C_{k_2} C_f \rho_l a_g a_l k_l$

$S_\epsilon = C_{\epsilon_2} C_f \rho_l a_g a_l \epsilon_l$

with C_f being an interphase friction coefficient as:

$C_f = \frac{3}{4}\frac{C_d}{d_b}|v_g - v_l|$, with

$C_D = \frac{8}{3}\frac{E_o}{E_o+4}$, where E_o is the Eotvos number defined as:

$$E_o = \frac{(\rho_l - \rho_g) g d_b^2}{\sigma_{l_q}}$$

It is worth noting that the bubble size is taken into account only in the friction coefficient.

The coupling between the continuous and the dispersed phase is done the interphase force M_i, found in the momentum equation. In the present study the drag force is the only interface force taken into account.

3.2.2. Imported geometry

The domain is resolved by a rectangular box. In the middle,two inlets are placed, representing the bubble screens. The geometry of the simulation is made identical to that of the experiment. Figure 3.4 depicts a domain of 2.4m length, 0.5 m wide and 0.4 m in height.

3.2.3. Boundary and Initial conditions

The initially at rest water, gets entrained in the water column, because of the injected air flow rate. Therefore the initial current velocity is set to zero. In addition, hydrostatic pressure is defined as an initial condition in the domain.

As far as the boundary conditions are concerned, the bottom, side and front walls are defined as wall boundaries, having the no-slip condition. The inlets are defined as velocity inlet boundaries. The volume fraction of the gas phase in the inlets is set to 1. A velocity is therefore required. This velocity is prescribed as follows:

$$u_{inlet} = \frac{Q_{air,total}}{2A_i}, i = 1,2$$

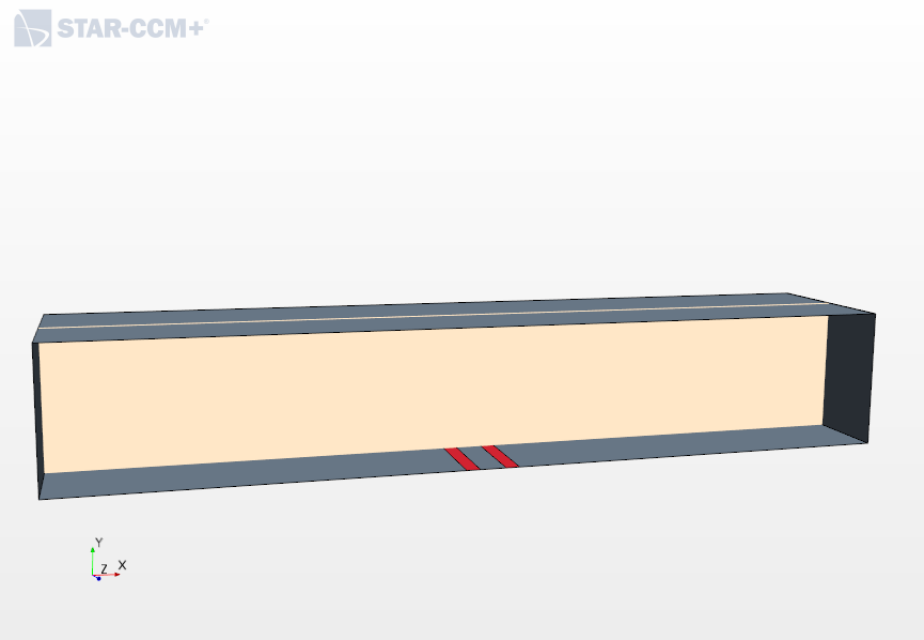

Figure 3.4: Imported geometry

It is already evident, how important the inlet velocity is. It is a single parameter, that defines how the gas phase in injected into the water.

Rigid lid assumption is made for the domain. The top boundary is defined as a permeable region for the gas phase to escape.

3.2.4. Mesh and CFL

The trimmed Cell Mesher is used with hexahedral cells. A refinement in the region near the bubble screen and the surface was sometimes prescribed. As a target, 8 cells per inlet were preferred to resolve with enough accuracy the flow. This was not always possible due to computational limitations.

A Courant number was targeted to 1 for numerical accuracy. However, this was also difficult to achieve.

The figures 3.5 and 3.6 indicate the mesh and Courant number in the domain in case of refinement.

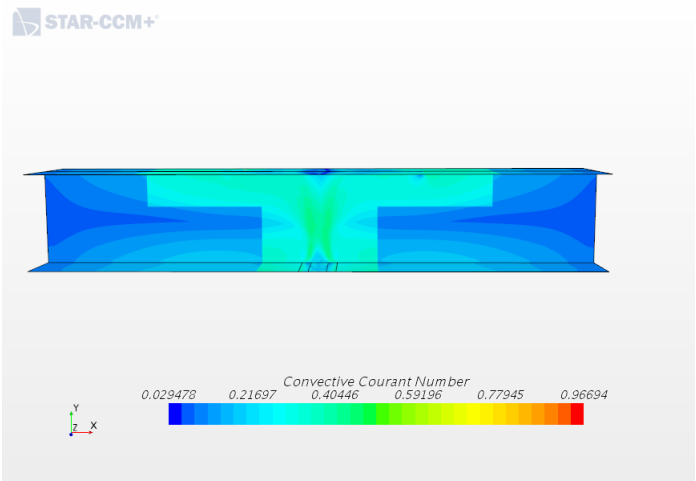

Figure 3.5: Courant number

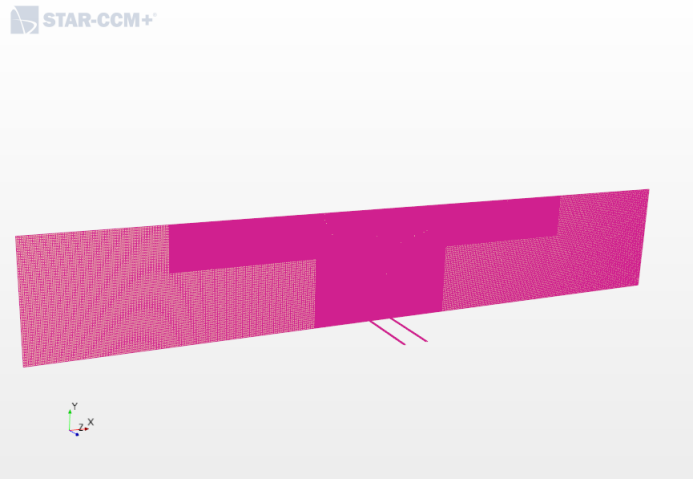

Figure 3.6: Trimmer mesh with refinement

3.2.5. Convergence and computational times

To achieve a converged solution, quantities of interest, in this case the mean velocities, are monitored in time. Since we are interested in the steady steady for the PIV measurements validation, a bigger initial time step is selected, which is then reduced to achieve a converged solution in the final steps.

The residuals are also an indication of convergence, in the sense that they express if the discretized equations are able to satisfy the solution at each time step.

The computational time need to achieve convergence, varies with mesh sizes and time steps. In the present study, for a mesh of approximately 200.000 cells and a CFL number close to 1, it takes approximately 1 day, whereas for a mesh of 7 million cells and a final time step of 0.001s, more than 5 days are needed. It is worth noting that 30 to 50 sub-iterations, are selected per time-step in the present study.

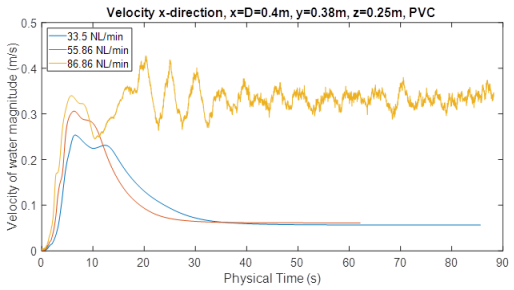

Figure 3.7: Velocity of water monitors. Cases with air flows rates 33.5NL/min and 55.86NL/min have converged to a steady state at 40s. In case with 86.86 NL/min velocity oscillates around a mean.

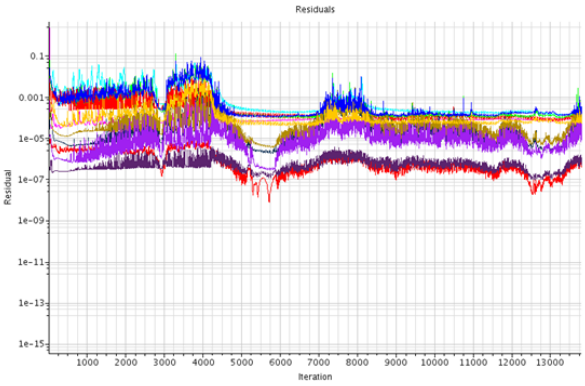

Figure 3.8: Residuals oscillate around a very small number

4

Results

4.1. Experimental results

Results of the PIV post-processing are in terms velocity profiles over a distance from the bubble screen. Additionally the three field of views (FoVs) are put together to represent the whole left side of the water tank, where the measurements took place. This can be found in Appendix A.

Next, the velocity profiles of the experimental results in distances equal to the height of the domain and two times the height of the domain will be presented. Special attention will be paid to the differences induced by the two bubble screen generators.

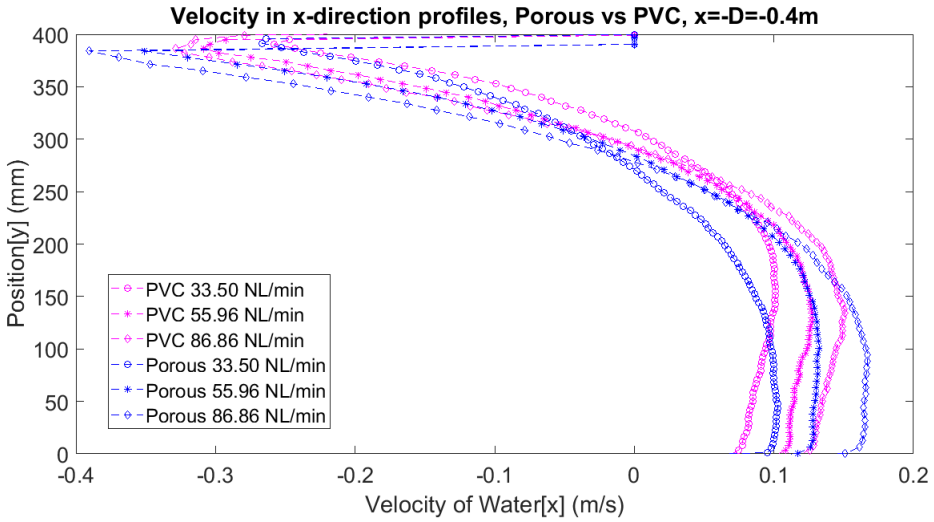

Figure 4.1: Experimental results in x=-D

Similar flow patters appear in all flow rates both the porous stones and for the PVC pipes (4.1). In the lower half of the water depth, a front of water appears, directed towards the bubble screen. In the top 15 cm the water gets deflected away from the bubble screen. In all cases, higher flow rates induce more mixing near the surface and also higher velocities near the bottom. The two different screen generators, result in not very different velocity profiles. More mixing near the surface is induced by the porous stones. However the bubble size created by the PVC pipes, are approximately 4 times larger.

Further away from the bubble screen lower velocity profiles are found, with the differences to be bigger for the PVC pipe. Mixing of the upper water column has decreased (4.2).

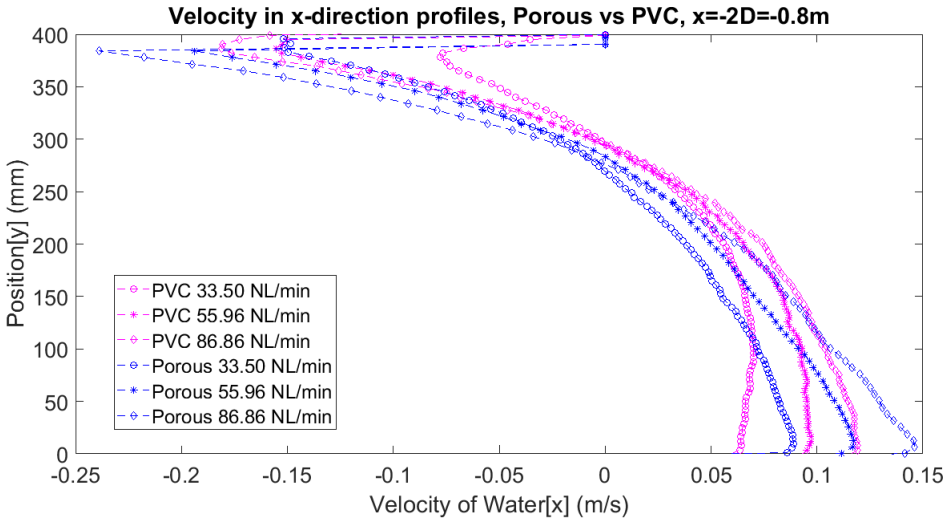

Figure 4.2: Experimental results in x=-2D

4.2. PIV vs CFD

In this section, the experimental results are plotted against the numerical ones. First, intermediate results are presented. This was a first attempt to simulate the experimental case. Afterwards, the efforts were concentrated in one air flow rate and on one bubble screen generator type.

Concerning the intermediate results an overview of the selected parameters is presented below. In this phase, efforts were concentrated on finding a converged solution for all the cases, with a relatively coarse mesh.

Model parameters	33.5 NL/min	55.96 NL/min	86.86 NL/min
No. of cells per inlet	8	8	8
Cell size	0.5cm/1cm	1cm	0.5cm/1cm
Total number of cells	232420	232420	407164
Δ t (s)	0.01	0.006	0.004
max CFL	1	0.6	0.8

Table 4.1: Overview of mesh and time specifications for the PVC bubble screen generator

Model parameters	33.5 NL/min	55.96 NL/min	86.86 NL/min
No. of cells per inlet	5	5	5
Cell size	0.5cm/1cm	0.5cm/1cm	0.5cm/1cm
Total number of cells	232420	232420	232420
Δ t (s)	0.01/0.001	0.01/0.001	0.01/0.001
max CFL	5	5	5

Table 4.2: Overview of mesh and time specifications for the porous stones bubble screen generator

The inlet area width in case of the PVC screen generator was 4cm equal to the diameter of the tubes. The width of porous stones was set to 2.5cm. The resultant velocity profiles are presented below.

It is clear from the comparison of the two, that the numerical model does not resolve the fluid dynamics of the phenomena. For both cases, the order of magnitude of the numerical results is significantly lower. However for the higher flow rate, the velocity profile has a larger magnitude and resembles a simple lock exchange test.

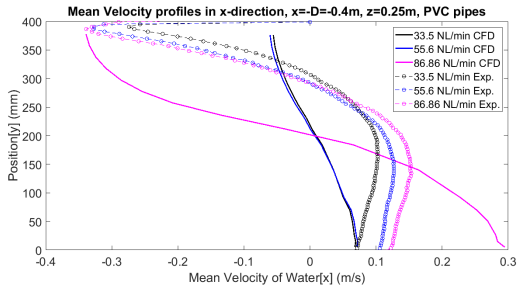

Figure 4.3: Experimental vs Numerical results for the PVC pipes

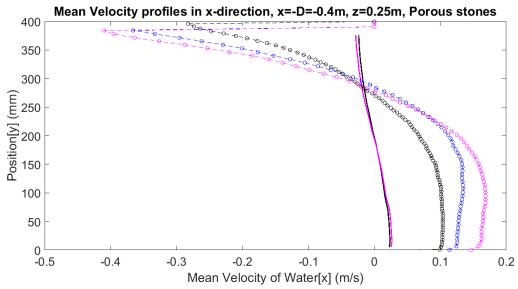

Figure 4.4: Experimental vs Numerical results for the porous stones

Following the previous results, it was decided that all the efforts would be concentrated on the higher flow rate of the PVC bubble screen generator cases. To that end, an investigation of a governing parameter was launched. The choice of the parameter was quite easy, because already from the previous phase,it was clear that the inlet model and the imposed velocity in the inlets is a strong factor. Other parameter that was considered to be of secondary importance is the choice of other turbulence model than the $k-\epsilon$.

The results that follow are also generated on a bigger mesh to be able to resolve more scales. In addition, other factors like the Eotvos number and the representative bubble size were defined more thoroughly.

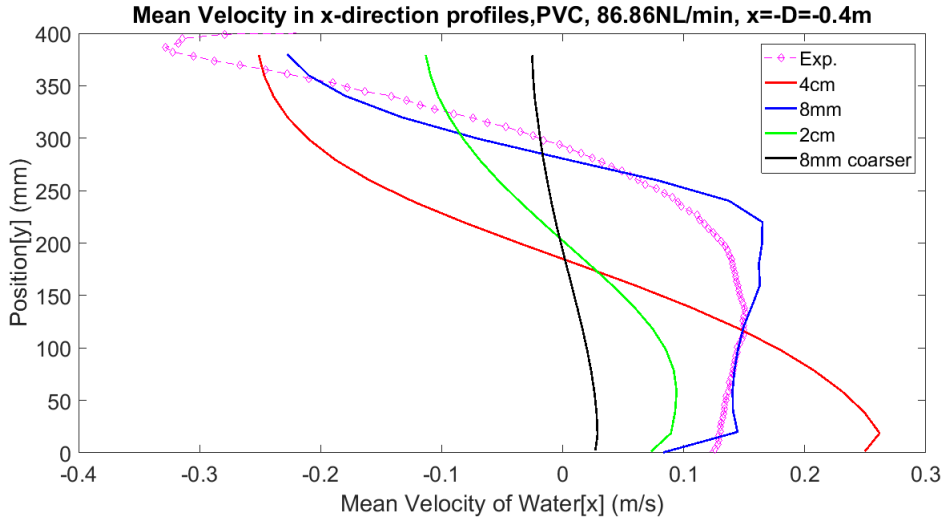

Figure 4.5: Numerical results for the PVC bubble screen generator and higher air flow rate with different inlet widths

It can therefore be concluded that the inlet model plays an important role in the results.

The initial 4cm inlet model and the 2cm inlet model are failing to reproduce the experimental results. The 8mm inlet model seems to perform a better job, except the region near the water surface. However it is a region with high uncertainty in the PIV measurements are well. That being said, it is concluded that the 8mm inlet model reproduces well enough the experimental results. It must be noted that the 8mm inlet is 10 times bigger than the holes of the PVC pipe.

The specifications for the numerical models are presented below.

Cases:	4cm	2cm	8mm	8mm coarser mesh
No. of cells per inlet	32	6.4	16	3.2
Cell size	1.25mm/2.5mm	1.25mm/2.5mm	1.25mm/2.5mm	2.55mm/5mm
Total number of cells	7514849	7514849	7514849	1888893
Δ t final (s)	0.001	0.001	0.001	0.002

Table 4.3: Overview of mesh and time specifications for the PVC bubble screen generator

5

Discussion

5.1. Relevance with already validated case

The numerical model of (Van Meerkerk and O'Mahoney, 2014), was able to succeed in reproducing the experimental results in a similar case as the one presented here. The authors used an inlet model that was not able to have the same results for the present study.

Despite the fact that the two cases had similar Fr_{air} numbers, important differences in geometry could lead to different governing physics. That being said, the height and with of the validated case, was significantly bigger. In addition higher air flow rates, led to higher injection velocities. In those higher velocities the CFD model is, for some reason, working better in resolving the physics. Out of the four cases computed in (Van Meerkerk and O'Mahoney, 2014), only the ones having similar inlet velocity as the ones of the present study, yielded bad agreement with the experiments.

5.2. Terminal velocity and bubble size

Following up, on the aforementioned statement that the CFD model is working better in resolving the physics for higher velocities, additional investigation was conducted.

Thanks to the study of *Haitsma Mulier et al.* project an equivalent bubble diameter for the PVC pipe cases is available. In their work, they determined the size of the bubbles entrained in water visually. From the equivalent bubble diameter, the Eotvos number used in the simulations and also the terminal velocity of the bubbles is defined with the help of the graph in 5.1.

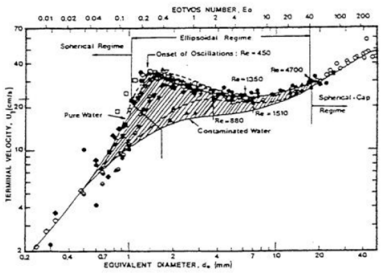

Fig. 6.19: Terminal velocities of air bubbles in water at 20°C. (from Grace and Wairgi, 1986).

Figure 5.1: Terminal velocity as a function of the equivalent bubble diameter. Source: Oliemans (1998)

All the above information are summarized in the table below.

[!h]

Low Fr_{air} number	Intermediate Fr_{air} number	High Fr_{air} number	
Equivalent bubble diameter (mm)	4.53	4.87	5.11
Eotvos number (-)	3	3.3	4
Terminal velocity (cm/s)	20	20	20

Table 5.1: Overview of mesh and time specifications for the PVC bubble screen generator

Next, a comparison of the terminal velocity with the inlet velocities from the numerical model will be addressed. In case of the intermediate results, which did not reproduce the experiments well, the inlet velocities are far below the terminal velocities. In (Van Meerkerk and O'Mahoney, 2014) case, the bubbles are injected almost from the beginning in the terminal velocities.

	Injection velocity cm/s			Terminal Velocity cm/s		
	low rate	medium rate	high rate	low rate	medium rate	high rate
PVC with 4cm inlet area	1,4	2,33	3,62	20cm/s-25cm/s		
PVC with 2cm inlet area	2,79	4,66	7,24			
Porous with 2,5cm inlet area	2,23	3,73	5,79	15 cm/s		

Table 5.2: Comparison of injection and terminal velocities for all the cases

Mike case	Injection velocity cm/s				Terminal,Velocity cm/s		
	low rate	medium rate	medium rate	high,rate	low rate	medium rate	high rate
2cm inlet area 4mm bubble size	3,4	12,3	24,1	57,6	20cm/s-25cm/s		

Table 5.3: Comparison of injection and terminal velocities for the validated case from literature

Finally, reducing the inlet area, the inlet velocity increases. In case of the 8mm inlet area, 10 times bigger than the orifices of the PVC pipe, the results showed better comparison with the experimental ones. For those cases, the terminal velocity of the bubbles is closer to the inlet velocities one as depicted below.

	Injection velocity cm/s			Terminal Velocity cm/s		
low rate	low rate	medium rate	high rate	low rate	medium rate	high rate
PVC with 4cm inlet area	1,4	2,33	3,62	20cm/s-25cm/s		
PVC with 2cm inlet area	2,79	4,66	7,24			
PVC with 8mm inlet area	13,96	23,31	36,19			

Table 5.4: Comparison of injection and terminal velocities for the various inlet models

5.3. Computational time

The last simulations, which used an inlet model with width 8mm and a total number of cells of about 7 million, needs more than a week to reach a steady state. Further reduction of the inlet width was intended, but this was not possible due to computational time limitations. That being said, because of the complexity of the multiphase flow solver, even more time was needed to make sure than the residuals of interest would indeed have reached a steady state.

6

Conclusions

In the beginning of this study, research questions were formed, aiming at further understanding bubbly induced flows and how they can be efficiently modelled by CFD. To facilitate that purpose, smaller questions of key importance were addressed and a methodological approach to answer them is presented, which led to the following conclusions.

The F_{air} number, used for scaling purposes, is not able to capture the main phenomena of bubbly driven flow and effectively translate them to different scales. It is missing a component directly related to the bubbles. This component could possibly be the bubble size. Alternately, for practical purposes, it could be a design parameter, for example the size of the orifices, which is related to the equivalent bubble diameter. (Mazijk, 1971) in his work, he introduced a dimensionless number more focused to the salt intrusion through a bubble screen, but it is not a practical one.

Modeling of bubbly flows is a complex process, as can already be seen from the large amount of previous work. When modeling bubble screens, depending on the physical scales of the problem, appropriate models have to be selected for the interphase forces between the continuous and the dispersed phase, and other physical effects.

The way the inlet is modelled, along with the mesh size, have a profound effect of the modelling results. In the present study, a minimum mesh of about 7 million was needed to resolve the scales of the flow. A coarser mesh could not reproduce the underlying phenomena.

The CFD model, appears to simulate the physics of the flow in a better way, if the terminal velocity of the bubbles is close to the one that is imposed in the inlet boundary. From literature and from experiments, it is expected that the bubbles within a short period from their generation point, are able to reach the terminal velocity. A hypothesis is formed within the current study, that this is a mechanism that the current CFD model cannot resolve or the height of 40cm used in the experiment, is not enough for the bubbles to develop in the CFD model. The supporting evidence that accompanies this hypothesis, is presented in the Chapter 5, but further research would help on estimating the its validity and accuracy.

7

Recommendations

Some ideas for further research in understanding how bubbly flows can be efficiently modelled using CFD, are presented in the following.

Firstly, in the present study an Euler-Euler approach was used. This method has the advantage of low computational cost compared to the Eulerian-Lagrangian approach, and was used as a first step. Nevertheless, an important drawback is the lack of physical detailed of the bubble dynamics and the carrier-fluid-bubble interaction. To that end Eulerian-Lagrangian approach is recommended as a next step. The work of Fraga et al. (2016) could provide a great source of information for this purpose.

Secondly, in stead of using a turbulence response model for the gas flow, the $k-\epsilon$ as a first approximation, can be used for the gas phase as well. Using a turbulence response model is a valid assumption for low gas volume fraction. When the air flow rate increases it cannot be used.

In addition, further refinement of the mesh is needed to achieve mesh independency. Due to computational power limitations, this could not be done within the present study.

Finally, following the last conclusion, further study could be conducted for the terminal velocity of the bubbles and their generation. Using slow motion videos, available from the PIV measuremets processing, it could be possible to track and measure the velocity of the entarind bubbles. This could also provide insight on the CFD modelling considerations.

Bibliography

Abraham, G. and van der Burgh, P. (1962). *Reduction of salt water intrusion through locks by pneumatic barriers*. Rijkswaterstaat, Service for Water Management.

Bulson, P. (1961). Currents produced by an air curtain in deep water. *The Dock and Harbour Authority*, 42(487):15.

Fraga, B., Stoesser, T., Lai, C. C., and Socolofsky, S. A. (2016). A les-based eulerian–lagrangian approach to predict the dynamics of bubble plumes. *Ocean modelling*, 97:27–36.

Keetels, G., Uittenbogaard, R., Cornelisse, J., Villars, N., and Pagee, H. V. (2011). Field study and supporting analysis of air curtains and other measures to reduce salinity transport through shipping locks. *Irrigation and drainage*, 60(S1):42–50.

Kurian, J. (2017). Post-Processing and analysis of measurements on bubble screens to mitigate salt intrusion. Technical report, Deltares.

Mazijk, A. v. (1971). Reproductie zouttoestand getijrivieren (xiii): Schaalonderzoek: resultaten proef t 164. *m0896*.

Oliemans, R. (1998). *Applied Multiphase Flows: TN 378*. Delft University of Technology.

Pietrzak, J. (2017). Lecture notes: Stratified Flows, TU Delft.

Shin, J., Dalziel, S., and Linden, P. (2004). Gravity currents produced by lock exchange. *Journal of Fluid Mechanics*, 521:1–34.

Star CCM+ (2018). *User Guide*. Siemens.

Uittenbogaard, R. (2009). Memo.

Van Meerkerk, M. and O'Mahoney, T. (2014). Developemt of a cfd model of an air curtain fot saltwater intrusion prevention.

Wen, J. and Torrest, R. S. (1987). Aeration-induced circulation from line sources. i: Channel flows. *Journal of Environmental Engineering*, 113(1):82–98.

Wieleman, V. (2017). PIV measurements of bubble screen. Technical report, Deltares.

A

Stitching the FoVs

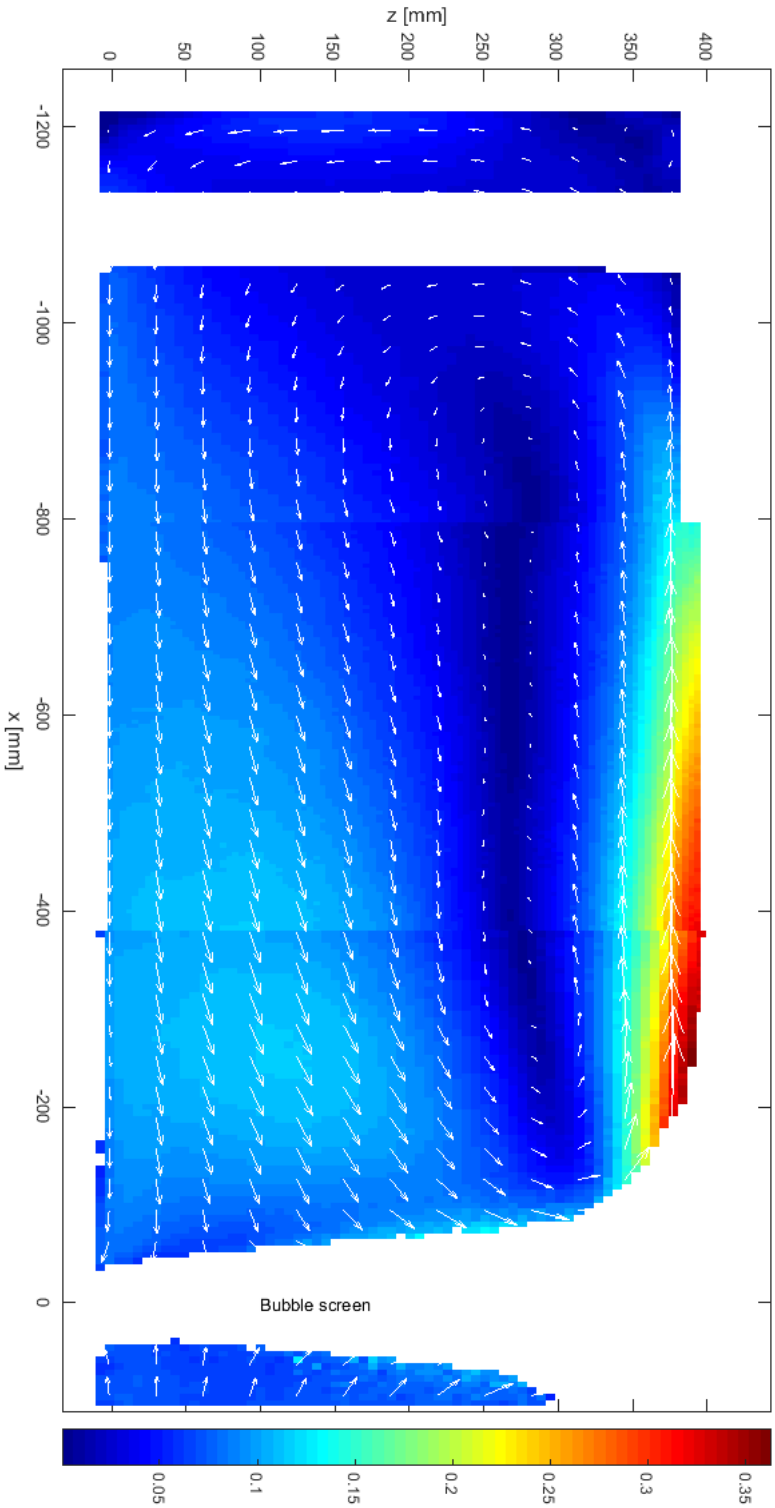

Figure A.1: Left side of the water tank with porous stones as screen generator and air flow rate of 33.50 NL/min

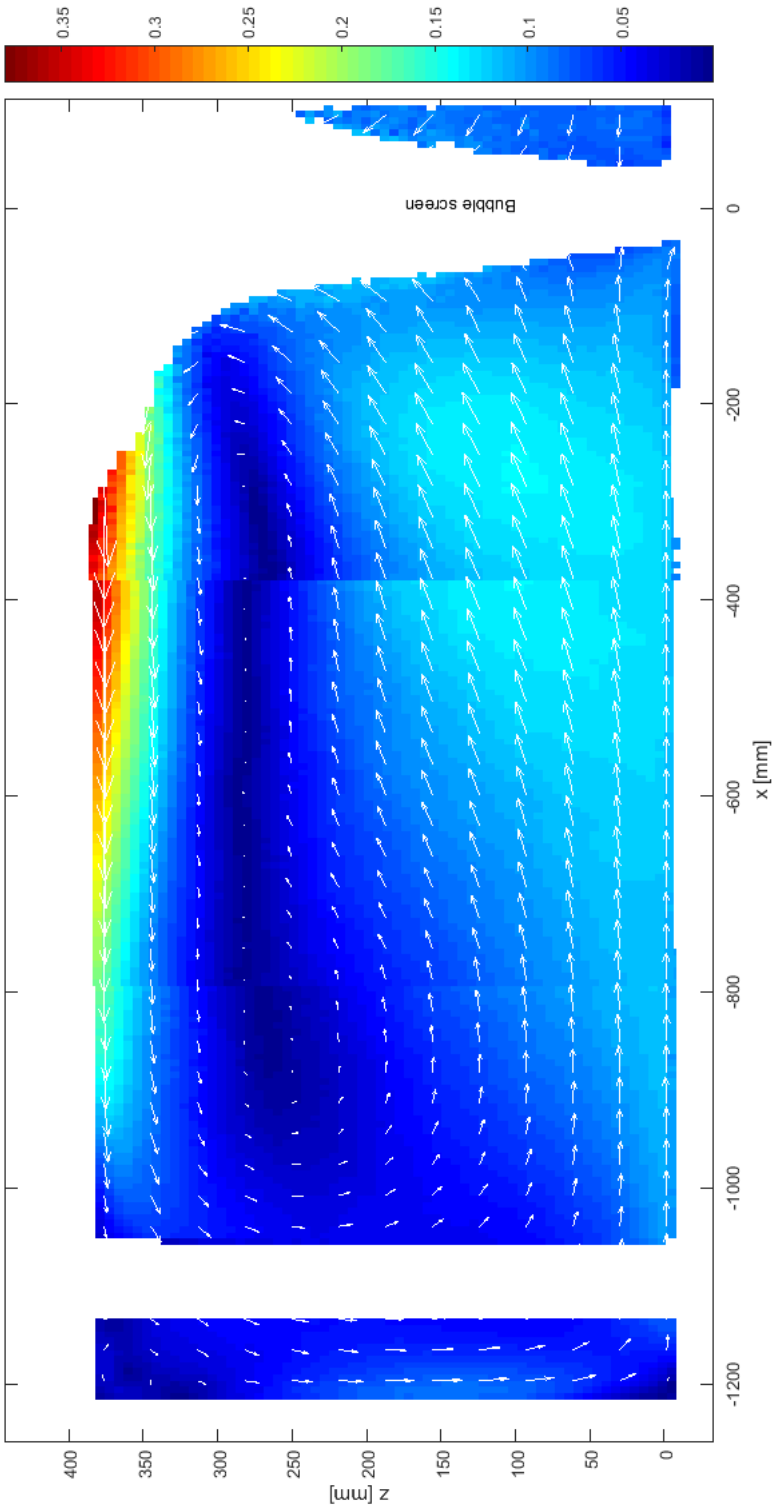

Figure A.2: Left side of the water tank with porous stones as screen generator and air flow rate of 55.96 NL/min

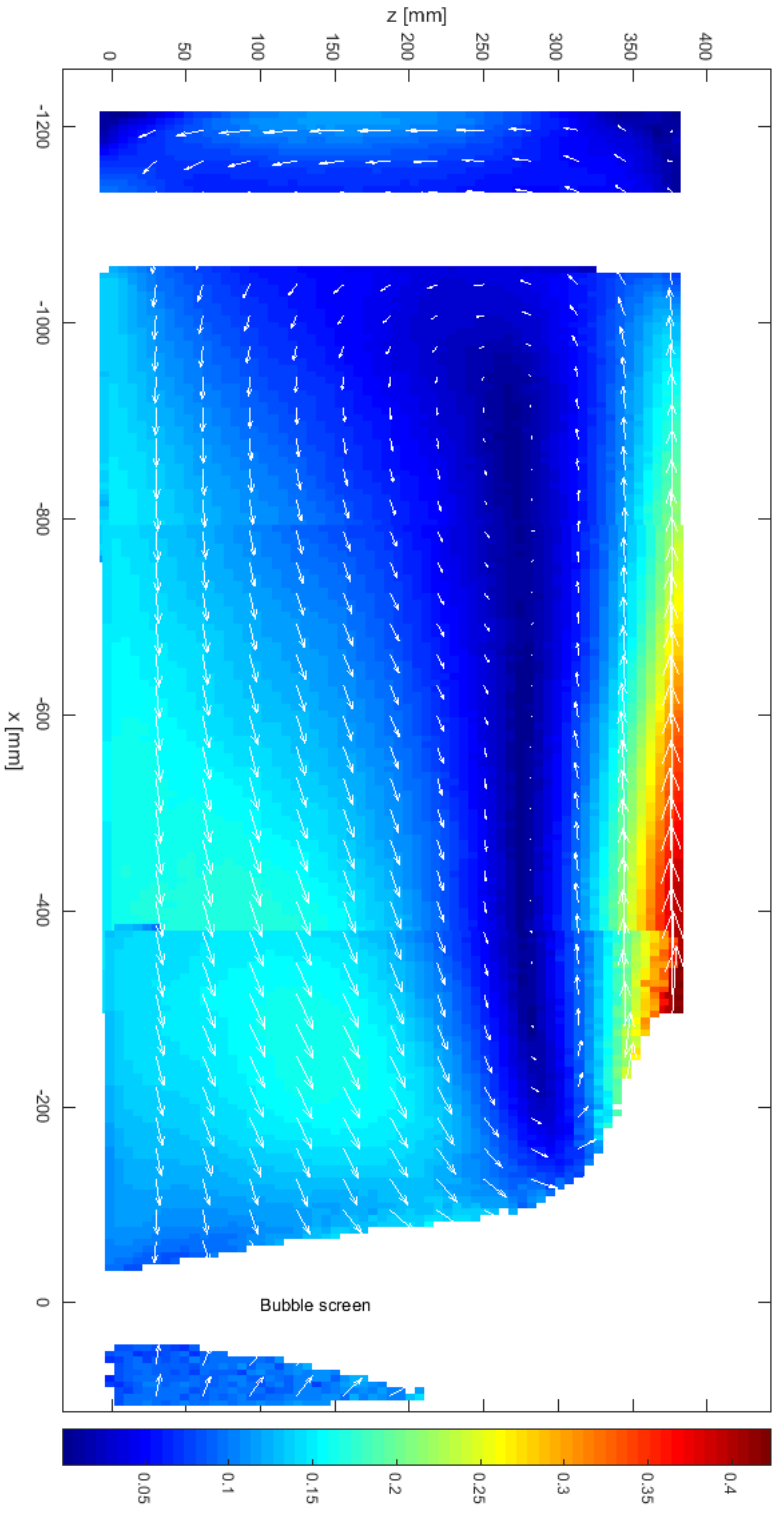

Figure A.3: Left side of the water tank with porous stones as screen generator and air flow rate of 86.86 NL/min

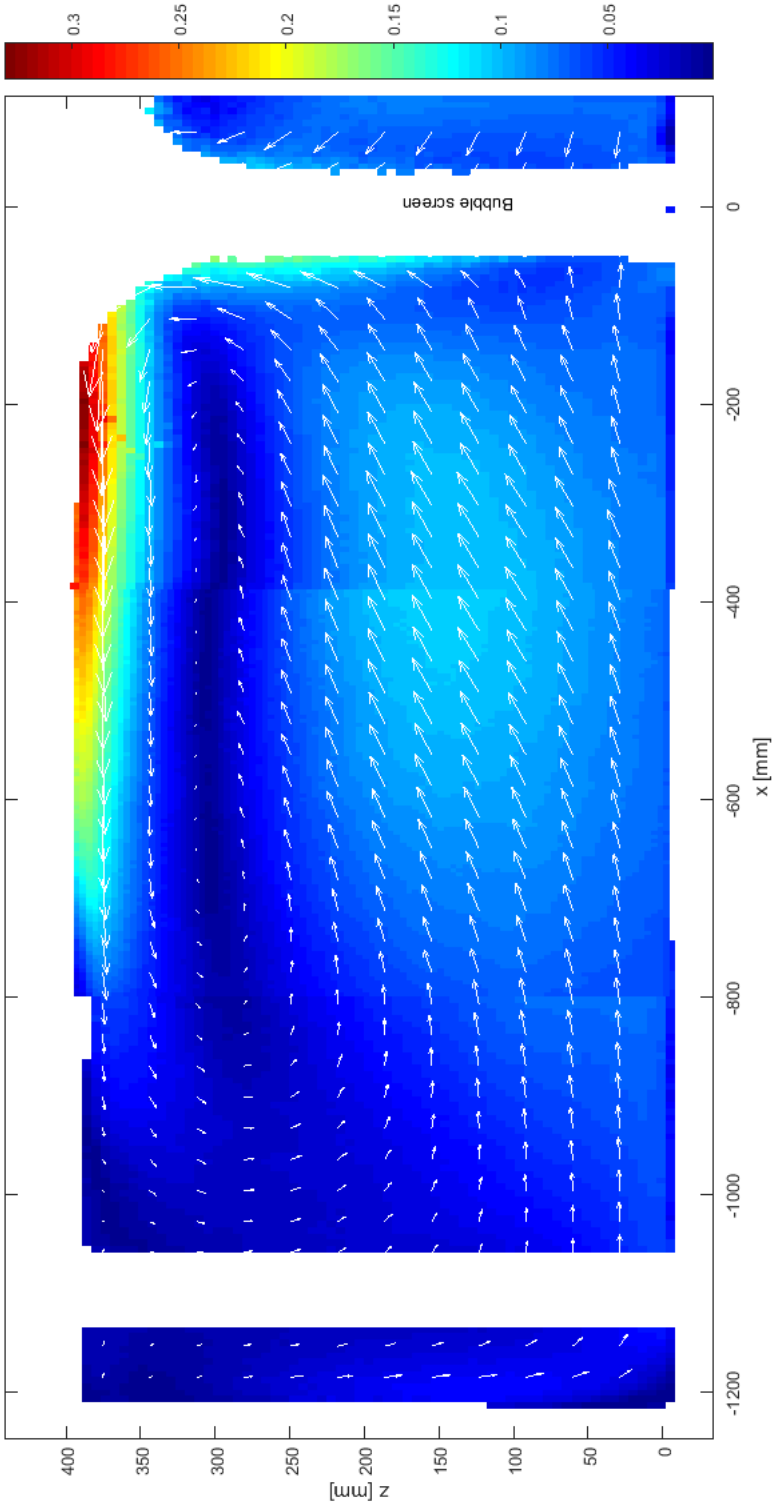

Figure A.4: Left side of the water tank with PVC screen generators and air flow rate of 33.50 NL/min

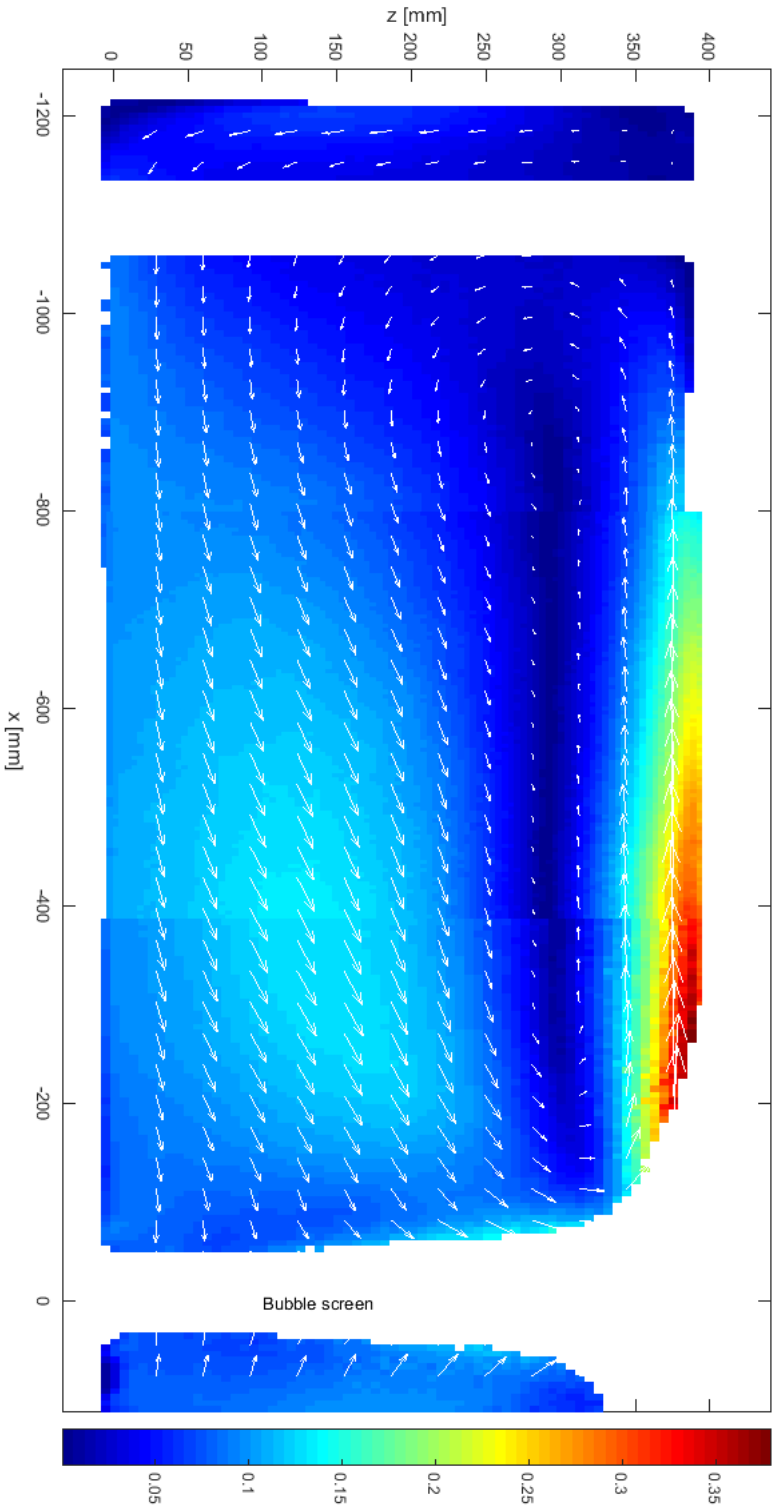

Figure A.5: Left side of the water tank with PVC screen generators and air flow rate of 55.96 NL/min

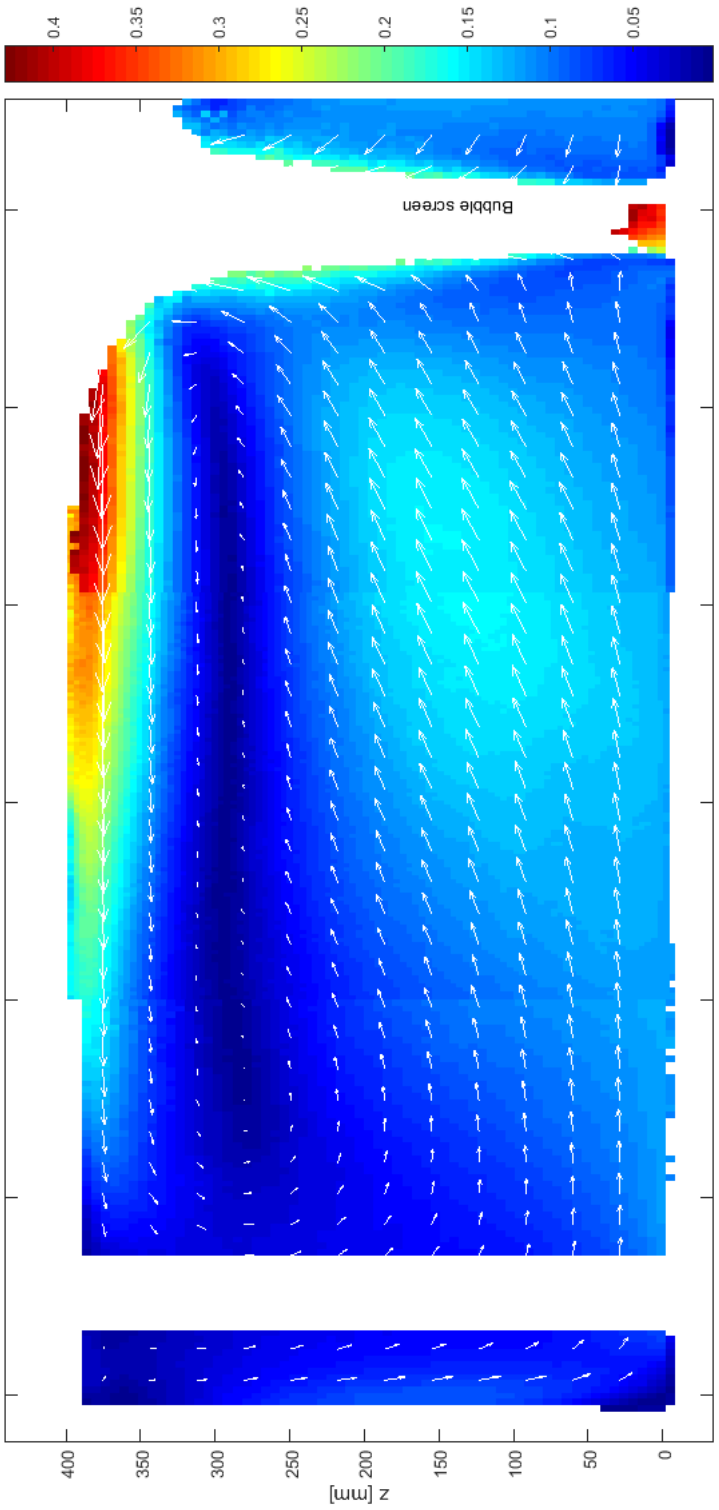

Figure A.6: Left side of the water tank with PVC screen generators and air flow rate of 86.86 NL/min